

Rossby Waves in the Southern Ocean: A Comparison of TOPEX/POSEIDON Altimetry with Model Predictions

C. W. Hughes

Proudman Oceanographic Laboratory, Merseyside, England

Abstract. Results are presented from an eddy-resolving model of the Southern Ocean which suggest that regions of moderate eddy activity are occupied by wavelike eddies with wavelengths of about 300 km and periods of 4 to 12 months. These waves travel eastward where the current (and wave amplitude) is strongest, and westward elsewhere, and it is argued that they are Rossby waves advected by the mean flow. It is shown that TOPEX/POSEIDON altimetry data should be able to resolve these waves in the Pacific sector of the Southern Ocean. A technique for wave detection is then presented which is capable of extracting useful information about the waves in this as well as other regions. Altimeter data are then presented which confirm the existence of waves in the Pacific sector and are consistent with wave presence elsewhere. An analysis of tide model errors shows that such errors are incapable of producing a signal which could mimic the modeled waves, although tide model errors may explain the difference between altimetry and model results in shallow regions of the ocean and in regions of low eddy activity.

1. Introduction

The Southern Ocean, especially the Pacific sector, is a region which has been very poorly sampled by oceanographic measurements. It is also unique in being a zonally unbounded ocean, a fact which makes Southern Ocean dynamics quite different from the dynamics of other ocean basins.

The Geosat altimeter (and to a lesser extent the short-lived Seasat mission) provided our first glimpse of the eddy activity in this energetic region, producing the now familiar maps of sea surface height (SSH) variability and inferred eddy kinetic energy (for example, *Chelton et al.* [1990] and *Shum et al.* [1990]), which showed very high energy regions associated with various topographic features, along with a band of moderate eddy activity roughly along the axis of the Circumpolar Current. The dynamical significance of this activity was quantified by *Morrow et al.* [1992] who calculated velocity variance ellipses and Reynolds stresses. This demonstrated that the eddies were often not isotropic, and in fact, acted to accelerate the eastward jets, in line with model predictions (for example, *McWilliams and Chow* [1981] and *Treguier and McWilliams* [1990]). In addition to acting in the wrong direction, they proved that Reynolds stresses are at least an order of magnitude too small to balance the eastward wind stress which acts at the surface, confirming that bottom form stress must be important in Southern Ocean dynamics.

The complex interaction between spatial and temporal sampling of the ocean surface by altimeters means that in order for a signal to be extracted from altimeter data, either its structure should be well defined (as is the case for tidal components), or it must have long intrinsic length and timescales. Neither of these factors is generally thought to apply to the ocean mesoscale eddy field, but results from the Fine Resolution Antarctic Model (FRAM) [*FRAM Group*, 1991] presented in section 4 show that much of the Southern Ocean eddy field takes the form of waves with coherence lengths and times long enough to render them detectable by altimetry given suitable processing. It is shown here that these waves can indeed be reconstructed using TOPEX/POSEIDON altimetry, and that the resulting reconstructions can provide useful dynamical information about the Antarctic Circumpolar Current.

2. Model Description

FRAM is an eddy-resolving, primitive equation model of the Southern Ocean south of 24°S, on a grid of one-fourth degrees in latitude by one-half degrees in longitude, with 32 levels in the vertical. It is based on the Bryan/Cox/Semtner code [*Cox*, 1984] and invokes the rigid lid approximation. This approximation allows the barotropic mode to be solved using a vorticity representation, thus permitting the model to be integrated without ever calculating absolute pressures, which means that the surface pressure fields necessary for comparison with altimetry must be calculated diagnostically, outside the main run (and must necessarily

Copyright 1995 by the American Geophysical Union.

Paper number 95JC01380.
0148-0227/95/95JC-01380\$05.00

be approximate, since the relaxation scheme used to solve for the barotropic mode yields horizontal pressure gradients which do not have precisely zero curl). This task was performed by S. Thompson of the Institute of Oceanographic Sciences, Deacon Laboratory, Surrey, England, who supplied 72 surface pressure fields diagnosed from the FRAM data dumps at monthly intervals, 48 of which are used here.

The model was spun up by relaxing the temperature and salinity values toward the *Levitus* [1982] climatology, while imposing an annual mean surface wind stress taken from *Hellerman and Rosenstein* [1983]. At the end of the sixth model year, the relaxation to Levitus was ceased except in the surface layer, where it is taken to represent surface heat and freshwater fluxes, and the winds were changed to climatological monthly values, again from *Hellerman and Rosenstein* [1983], with a linear interpolation between each pair of values. It is from this "free-running" period that the 48 surface pressure fields are taken.

The forcing of the model leads to a number of limitations. The monthly mean wind stress means that there is too little forcing, and therefore very little activity, at higher frequencies. Since the signals we will be looking at here are at lower frequencies, this makes them easier to pick out in FRAM data than in reality, as the background noise is underrepresented in FRAM.

The representation of heat and freshwater fluxes by a surface relaxation to Levitus and also the rigid lid approximation (see *Greatbatch* [1994] for a discussion of this) means that steric changes in SSH due to the seasonal cycle will be very poorly represented in FRAM. In addition, the bias of the Levitus data set toward summer values means that FRAM produced no Antarctic bottom water. As a result, the gradual erosion of density gradients by the eddy field produced a slow spin-down, with the volume flux through Drake Passage decreasing from about 188 Sv to 180 Sv over a 6-year period ($1\text{ Sv} = 10^6\text{ m}^3\text{ s}^{-1}$). This flow compares with observed values of typically 134 Sv [*Nowlin and Klinck*, 1986] and is in line with other modelled values such as approximately 200 Sv from *Semtner and Chervin* [1992]. Apart from effects directly related to this lack of bottom water formation, heat fluxes diagnosed from FRAM are in generally good agreement with current beliefs [*Saunders and Thompson*, 1993], which is encouraging evidence that eddies in FRAM are doing the right thing.

In addition to the above, some differences between FRAM data and reality should be expected from the representation of topography, which was smoothed to a scale of approximately 1 degree (Plate 1a) in order to avoid instabilities. Nonetheless, although there are differences in detail [*Stevens and Killworth*, 1992], SSH variability from FRAM (Plate 1b) is very similar to observations from Geosat, and the band of high variability clearly corresponds with the core of the Circumpolar Current (shown in Plate 1c). The momentum balance of FRAM also shows that eddies act to accelerate the eastward jets (D.P. Stevens and V.O. Ivchenko, The zonal momentum balance in a realistic eddy resolving

general circulation model of the Southern Ocean, submitted to *J. Phys. Oceanogr.*, and *Killworth and Nanneh*, [1994]) and the wind stress is predominantly balanced by bottom form stress, in agreement with deductions from Geosat. Despite the limitations of FRAM, this agreement augurs well for the predictive power of FRAM with respect to at least the qualitative features of the eddy field.

3. Processing of Altimeter Data

Rossby waves depend for their existence on changes in the Coriolis parameter (the beta effect), which interacts only with meridional velocities. For this reason the wavelike features seen in FRAM (see next section) are most clearly visible in the meridional velocity or in the zonal gradient of SSH. This is the quantity which was extracted from the altimeter data.

The disadvantage of this approach is that values can only be determined at altimeter crossover points (points where ascending and descending passes of the altimeter cross, Figure 1), since gradients can only be determined along the altimeter track, and two components are needed in order to extract the zonal gradient. If both passes are near to meridional, determination of the zonal gradient will be very sensitive to errors, making this method unsuitable for regions near the equator. The low inclination of the TOPEX/POSEIDON orbit (approximately 66°), however, means that the amplification of errors in the Southern Ocean is reasonably small, although the opposite is the case for meridional gradients. A thorough examination of these issues, and of their interaction with the temporal sampling, is given by *Morrow et al.* [1994]. In the present case, where the gap in time between the two passes is never longer than 5 days, the lack of coincidence is not a problem, but it can become a problem for satellites with a longer repeat period.

The chief advantage is an insensitivity to long wavelength errors; the differentiation of SSH implicit in looking at slopes amplifies short wavelength signals relative to longer wavelengths. Since the chief sources of error in altimetry (orbit error, tides) are at wavelengths of several thousand kilometres or more, this gives slopes an advantage over heights in detecting these signals. Errors in tide models in particular, have made unambiguous identification of Rossby waves very difficult using SSH [*Schlax and Chelton*, 1994].

TOPEX/POSEIDON data from the merged Geophysical Data Records (GDR-M) [AVISO, 1992] were read, and sea surface heights relative to the OSU91A geoid [*Rapp et al.*, 1991] calculated using the Centre National d'Etudes Spatiales (CNES) orbits, which have been estimated to have a radial accuracy of about 2.5-cm root-mean-square [*Novel et al.*, 1995]. The usual path length corrections were applied (modelled atmospheric pressure "dry" correction, radiometer-measured water vapour "wet" correction, ionospheric correction from the dual-frequency altimeter when TOPEX was in operation, from Doppler orbitography and radioposi-

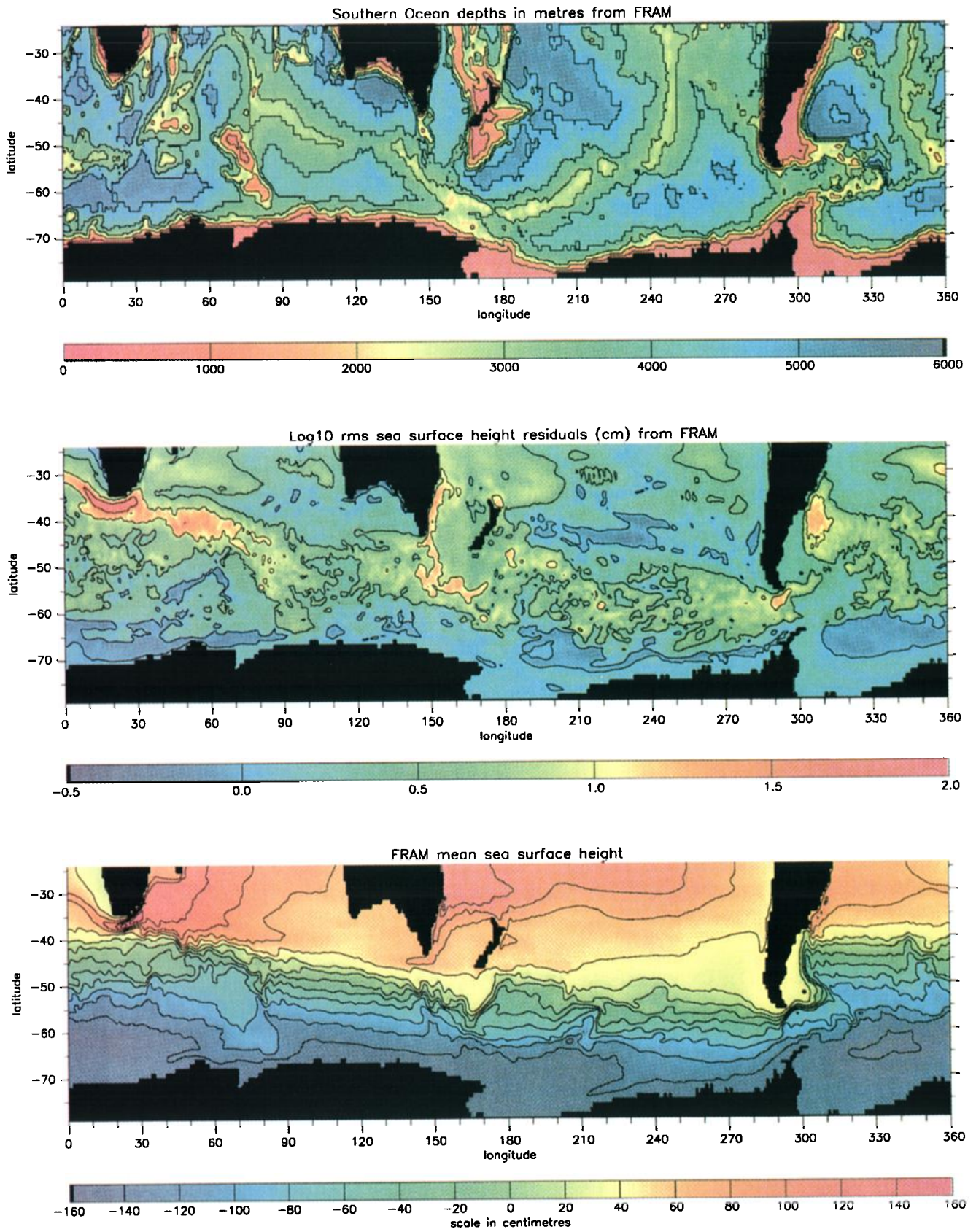


Plate 1. The Southern Ocean as represented by FRAM, (a) bottom topography, (b) sea surface height variability on a logarithmic scale, (c) 6-year mean of sea surface heights.

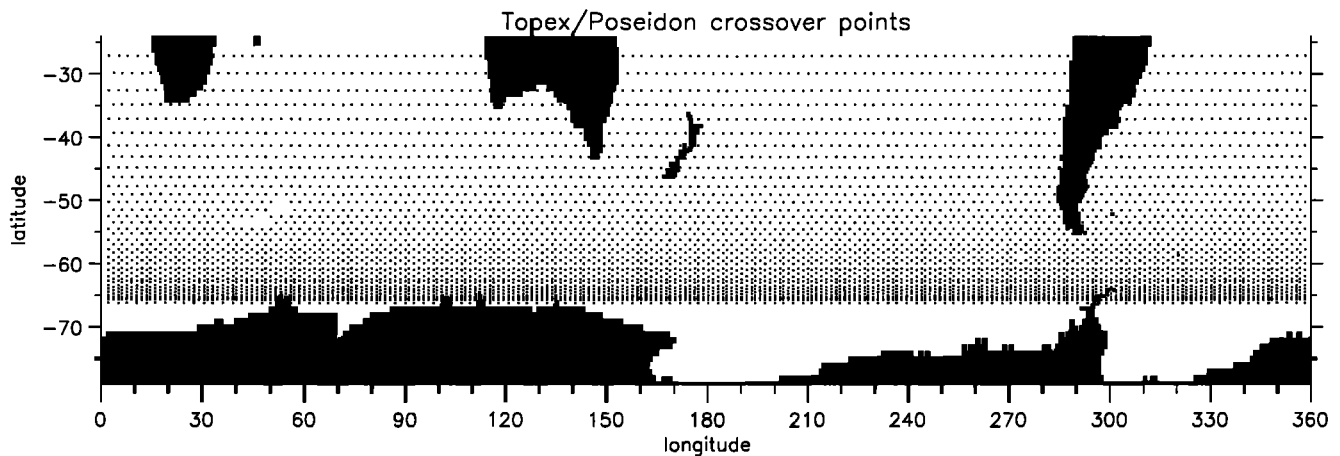


Figure 1. TOPEX/POSEIDON crossover points in the Southern Ocean.

tioning integrated by satellite (DORIS) tracking when POSEIDON was on), the inverse barometer correction was used, and tidal corrections for Earth and pole tides and the *Cartwright and Ray* [1991] model for the elastic ocean tide were taken from the CD-ROMs. The electromagnetic (EM) bias values were calculated according to the formula of *Gaspar et al.* [1994] as recommended in the AVISO user handbook. The resulting sea surface heights were linearly interpolated onto a set of latitudes with approximately constant along-track spacing of 7 km. A mean value at each point was calculated from 36 cycles of data starting with cycle 11, since earlier cycles have a slightly degraded accuracy due to a satellite mispointing error. This mean represents approximately 1 year beginning on December 31, 1992. This mean was subtracted, and the resulting residuals from the 48 cycles, numbers 5 to 52, (November 1, 1992, to February 20, 1994) form the data set from which crossover values were calculated. Forty-eight were chosen as a convenient number for input to a fast Fourier transform, with cycle 52 being the last one available at the time of writing. It was felt that the slightly degraded accuracy of cycles 5 to 11 was outweighed by the advantages of a longer time series. In calculating the means, both TOPEX and POSEIDON values were used with a relative bias of 16 cm (TOPEX measures longer than POSEIDON) consistent with the EM bias formulation used [AVISO, 1992, Appendix B], and mean values were only calculated where at least 20 cycles were present. This is not a crucial factor in the following work which is only considering deviations from the mean of sea surface slope.

For each cycle the ascending passes were used as a reference, and crossovers were calculated from these ascending passes and whichever descending passes were closest in time (no more than 5 days apart). The crossovers for cycle 14, for example, consisted of data from the ascending passes from cycle 14, and descending passes from cycles 13, 14 and 15. The exact latitude of the crossover was found by linear interpolation of the satellite position (assuming locally Cartesian coordinates), and a quadratic was fitted to the patch of

12 SSH residuals surrounding this latitude, with along track distance as the independent variable. Residual heights departing by more than 10 cm from this fit were discarded and the fit repeated iteratively until either, no points were more than 10 cm from the fitted curve or, fewer than six points or only points on one side of the crossover were left. In this latter case the crossover was discarded as a bad point. From these fits, which encompass a distance of about 77 km around the crossover point, the along-track slopes were calculated at the crossover. From the two along-track slopes, the zonal slope was calculated from $S_z = (S_a + S_d) / \sin \theta$, where S_z is the zonal slope, S_a is the along-track slope on the ascending (northward travelling) pass, S_d is the along-track slope on the descending (southward travelling) pass, and θ is the angle between the altimeter track and north ($0 < \theta < \pi/2$).

Where either of the along track slopes involved is a bad point, the zonal slope will be missing. If a value is missing for one repeat cycle of the altimeter, but values are available for the cycle before and after, the missing value is filled by the average of the surrounding values. Other missing values are set to zero.

Having calculated the zonal slopes, a time mean value (excluding points set to zero) was calculated for each crossover point, and subtracted off. The resulting residual zonal slopes form the data set used in the following analysis. The root-mean-square value for each crossover point is shown (Figure 2), with above-background levels of activity again at the core of the Circumpolar Current. Typical values in the moderate activity band are about 2 microradians, or 20 cm per 100 km, a value well above expected errors due to tides or other corrections.

4. Model Results

Figure 3a shows a snapshot of the residual zonal gradient of SSH from FRAM day 4717. The moderate activity regions are seen to be occupied by wavelike structures with wavelengths of about 270 km (the apparent variation of scale with latitude is mostly produced by

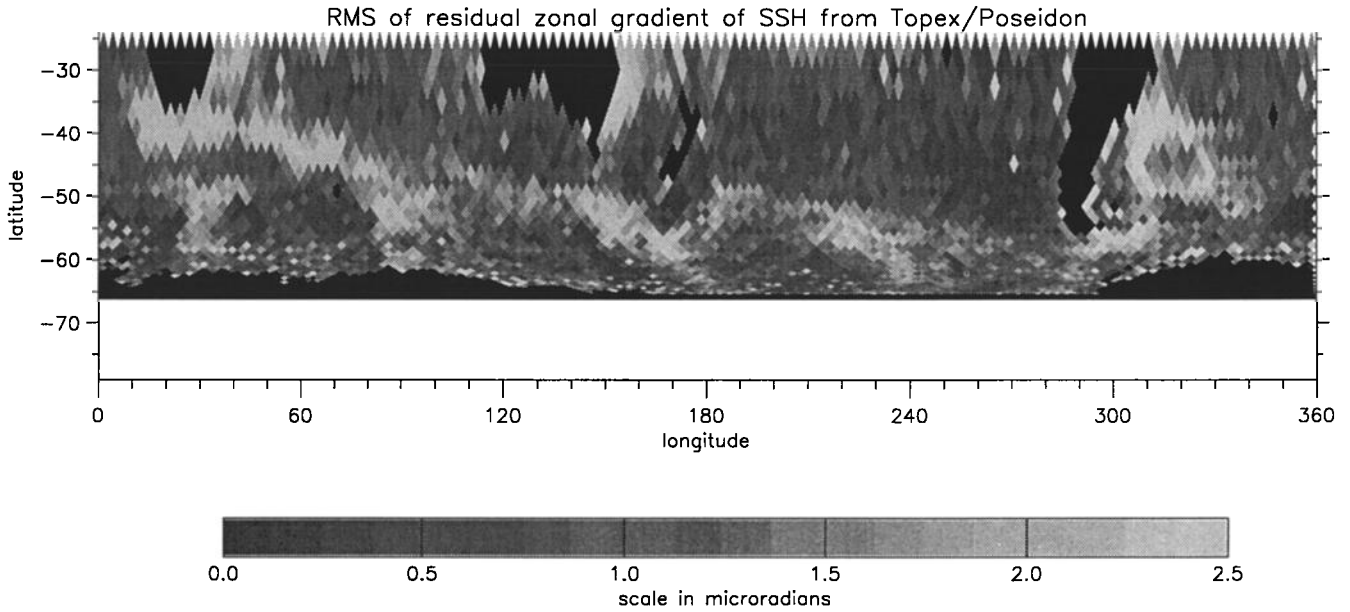


Figure 2. Root-mean-square variability of the zonal gradient of sea surface height, calculated from TOPEX/POSEIDON altimetry, cycles 5 to 52.

the projection used) and coherence lengths of order 15 degrees (about 750 km or 3 wavelengths).

This sort of length-scale may be derived in two different ways. For Rossby waves over topography in a stratified fluid (see *Rhines* [1970]), there is a surface-trapped mode which has a node approximately at the bottom. Flows in rotating stratified media obey a natural scaling (see for example *Gill* [1982], section 12.8)

$$\frac{NH}{fL} = 1, \quad (1)$$

where N is the Brunt-Väisälä frequency, f is the Coriolis parameter, H is the vertical scale, and L is the horizontal scale of the disturbance. Setting H to 5 km (the depth of the ocean), N to 10^{-3} s^{-1} (a value appropriate to the Southern Ocean), and f to 10^{-4} s^{-1} (the value at about 45 degrees) produces a horizontal scale of 50 km or, multiplying by 2π , a wavelength of about 310 km.

Nondivergent, zonally propagating Rossby waves in a uniform eastward flow of speed U obey the dispersion

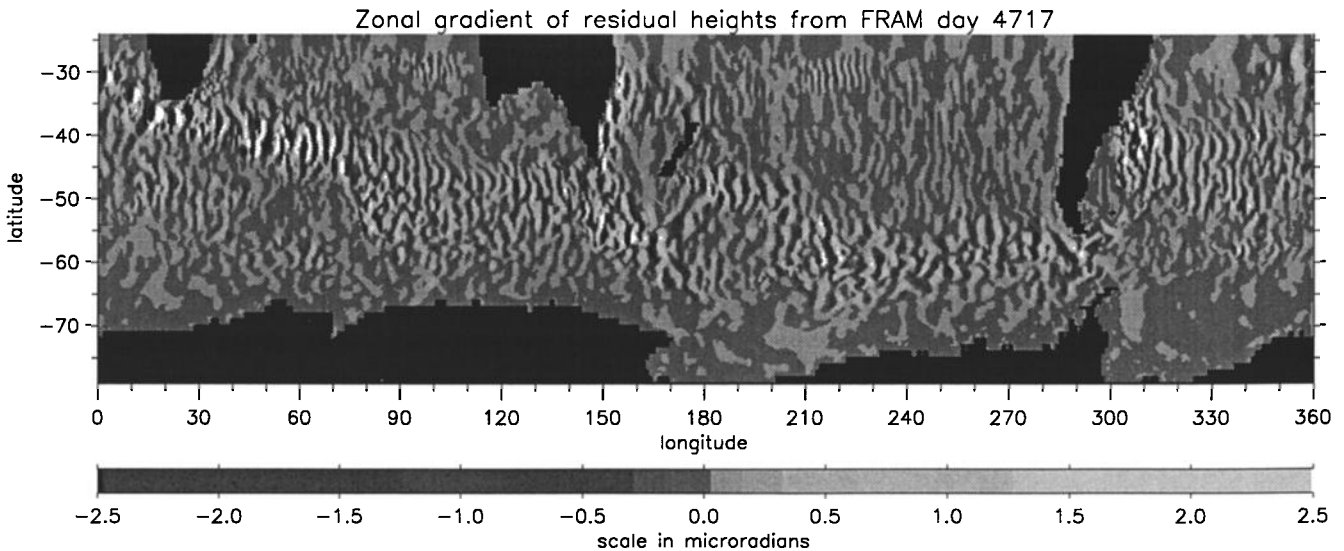


Figure 3. Snapshots of residual zonal gradient of sea surface height in the Southern Ocean, (a) FRAM day 4717, (b) approximate reconstruction of FRAM day 4717 from a local complex principal component representation of the data (see text), (c) similar to 3b but reconstructed from FRAM data sampled only at TOPEX/POSEIDON crossover points, (d) the same as 3c but using TOPEX/POSEIDON measurements to produce the principal components, and reconstructing the field for early February 1993.

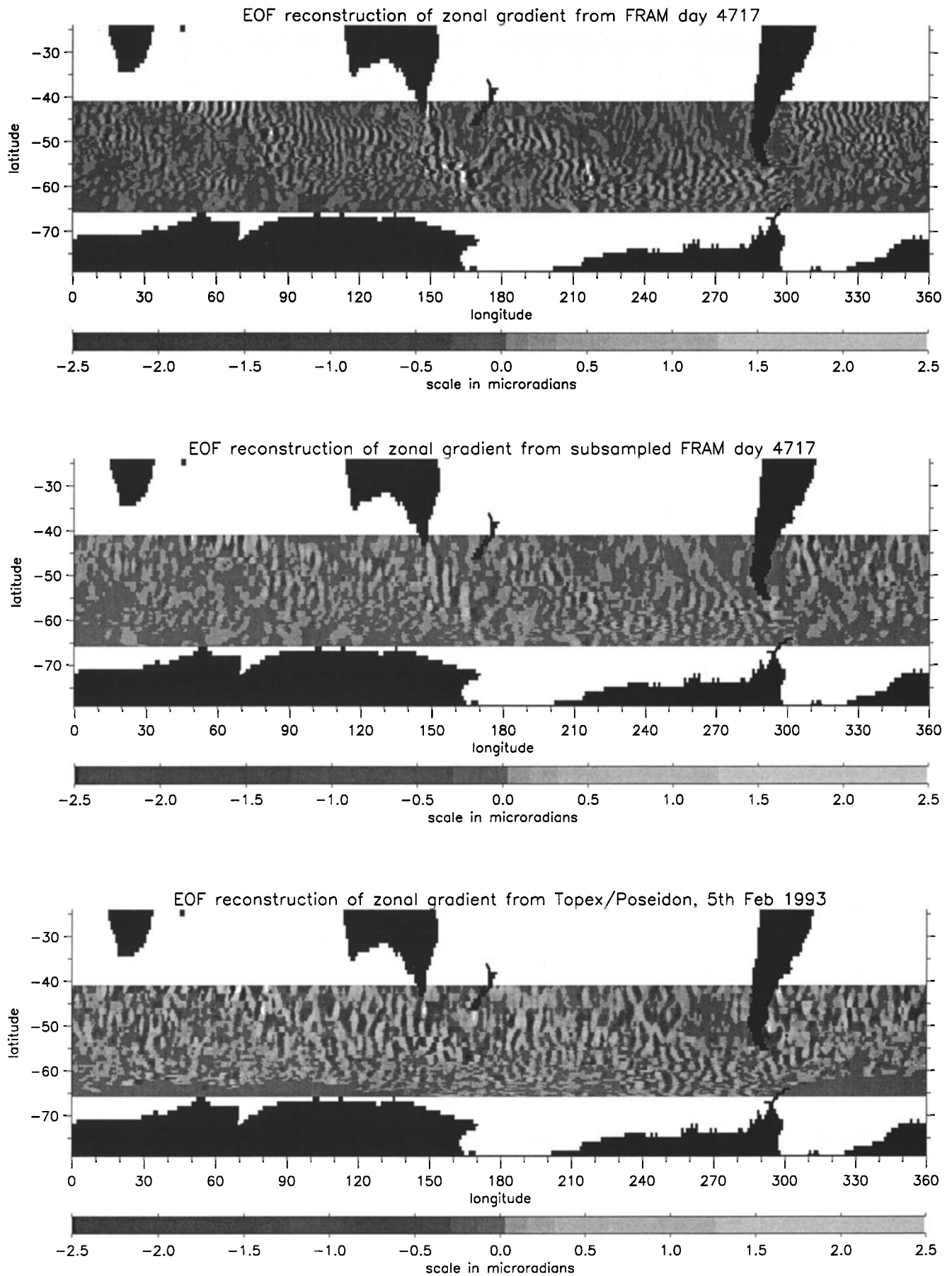


Figure 3. (continued)

relation

$$c = \frac{\omega}{k} = U - \frac{\beta}{k^2}, \quad (2)$$

so stationary waves are possible when $k = (\beta/U)^{1/2}$, or wavelength $\lambda = 2\pi(U/\beta)^{1/2}$. A flow of 200 Sv passing through a 1000 km by 4-km slice of the ocean represents a mean flow of 5 cm s^{-1} giving, for $\beta = 2 \times 10^{-11} \text{ m}^{-1} \text{ s}^{-1}$, a wavelength $\lambda = 2\pi \times 50 \approx 310$ km. Clearly, the observed waves are at a wavelength we would expect to see for Rossby waves in the Southern Ocean.

Both estimates of length-scale are very rough; the full situation is much more complicated with vertical shear of the mean flow (and also significant horizontal shear in some places). This can result in very complicated behaviour, particularly when the mean flow speed at some depth matches the wave phase speed (see for example *Gill* [1982], section 12.9). The detailed dynamics of such waves are beyond the scope of the present study, and U is merely supposed to be some kind of effective advection velocity which the wave feels. The simple vertical structure of the modelled waves makes the idea of some sort of "steering level" velocity seem credible.

A zonal section of a wavelike region in the Pacific sector (Figure 4) shows that the waves are indeed surface-trapped, decaying to a much smaller amplitude at the bottom of the ocean. The phase tilt, if any, is most often eastward with height, indicating that the waves probably do not develop in situ (a disturbance growing by baroclinic instability must have a westward phase tilt with height, see *Gill* [1982], chapter 12) but more likely are radiated from local regions of instability.

Animation of model results clearly shows that the waves in the core of the Circumpolar Current move eastward while other regions (especially in the Pacific and Indian oceans) contain westward moving waves with lower amplitudes. A time/longitude section (Figure 5a) shows eastward velocities of between 5 and 15 degrees per year (about 1 to 3 cm s^{-1}), which is slower than the mean flow speed. This difference, and the fact that the eastward propagating waves occur in the

region of higher than average eddy activity, suggests that the Southern Ocean can usefully be divided into two dynamical regimes in which the strength of the mean flow is, respectively, subcritical and supercritical with regard to the speed of propagation of natural-scale Rossby waves: in one region relatively low-amplitude waves have westward phase propagation, whereas in the core of the Circumpolar Current, higher-amplitude waves are advected eastward by the strong mean flow.

5. Principal Component Analysis

The relatively short coherence lengths of the waves in both space and time mean that Fourier analysis can only identify the wavelengths and periods very roughly and the phase speed, although clearly defined in Figure 5a, would be very poorly constrained. In an attempt to find an objective way of extracting these parameters from the data, a method involving localised complex principal components was developed.

The Fourier transform of a real time series has Hermitian form, with negative frequency components being the complex conjugate of the equivalent positive frequency component. The inverse transform is thus effectively a sum of standing waves, producing the original time series. If the negative frequency components are instead set to zero and the positive components doubled, the real part of the inverse transform is again the original time series, but it is accompanied by an associated imaginary part which results from the transform being effectively a sum of travelling waves. If complex time series are synthesized in this way from the real time series produced at a number of different places, complex principal components (CPCs) can be derived from the synthesized data set. See *Barnett* [1983] for a more complete description of CPCs.

The advantage of this is that a single CPC consists of a complex function of time, T , and an associated complex function of space, X , and can therefore represent a travelling disturbance. Real principal components must represent a travelling wave as a sum of two standing waves.

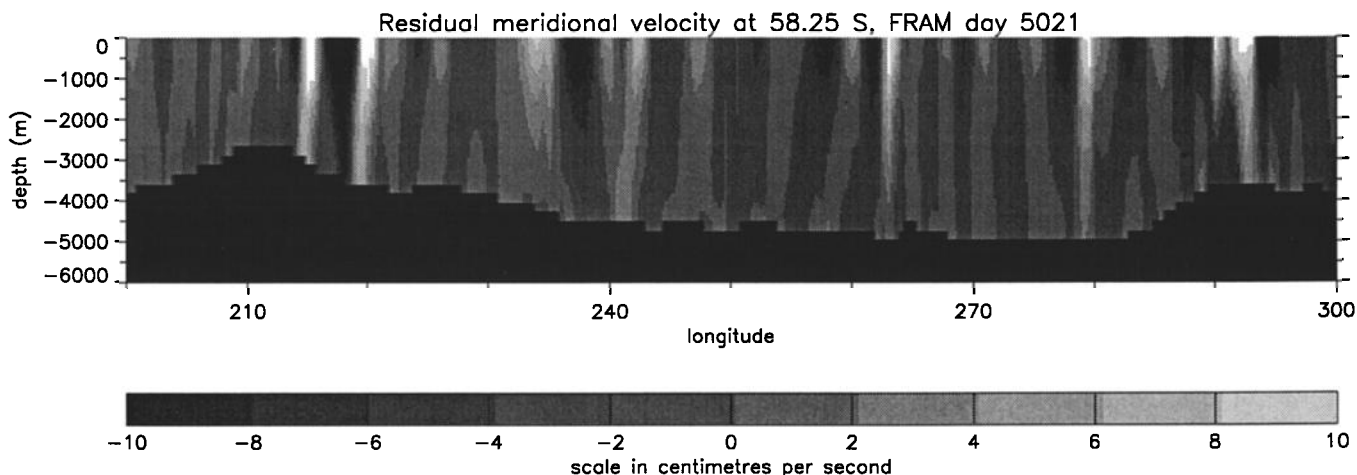


Figure 4. Snapshot from FRAM of the residual meridional velocity along 58.25°S , showing the vertical structure of the Rossby waves.

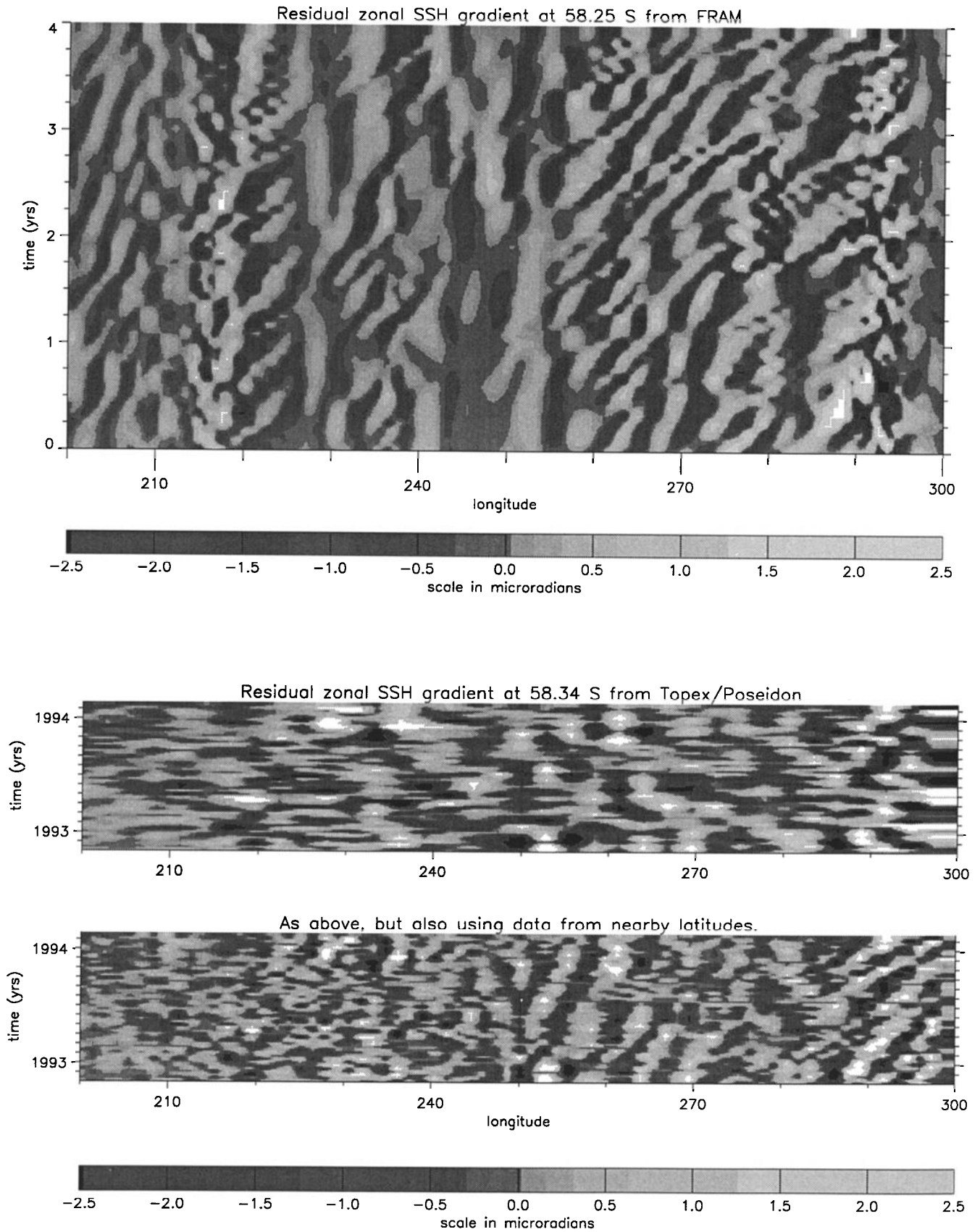


Figure 5. Time/longitude section of residual zonal gradient of sea surface height (a) from FRAM, at 58.25°S, (b) from TOPEX/POSEIDON altimetry at crossover points along 58.34°S, (c) the same as 5b, but also using altimeter data from the two neighbouring crossover latitudes, interpolated to the central latitude.

In the case of a disturbance which consists of several wave packets, each with the same wavelength, passing through a region, such a disturbance can be represented by a single CPC as

$$P = XT, \quad (3)$$

where

$$X = A(x) \exp(ikx) \quad (4a)$$

$$T = B(t) \exp[-i(\omega t - \phi_n)], \quad (4b)$$

and A , B are real. B is zero between wave packets and ϕ_n is a reference phase which can be different for each wave packet. Estimates of ω and k can be derived from

$$\omega = -\frac{d}{dt} \arg(T), \quad k = \frac{d}{dx} \arg(X). \quad (5)$$

If mean values are calculated, A and B can be used as weighting factors to avoid incorporating into the mean random phases due to small amplitudes. The resulting values of ω and k will then give a good representation of $c = \omega/k$, the phase velocity of the disturbance. Deviations from the mean of the weighted values of ω and k will give an idea of the quality of fit: large deviations mean that the component is poorly represented by (4).

For the FRAM data, time series were extracted for patches 33 grid points (16.5 degrees of longitude) long, along each latitude. In the following plots, each patch is only associated with the central 11 grid points (patches overlap so each section of 11 grid points is at the centre of one patch). The first CPC was calculated for each patch, and a time series reconstructed from just that component. Figure 3b shows a snapshot of the reconstructed field for the same time as Figure 3a, demonstrating how well the first principal components represent the wave motion. Wave parameters were then derived from each of these first CPCs, and are shown in Plate 2a. Note that this and several other figures only show a subregion of the FRAM area between 41°S and 66°S. This is because the TOPEX/POSEIDON orbit does not reach farther south than 66°S. North of about 40°S the latitudinal separation of crossovers becomes too great for resolution of waves at these wavelengths (see section 6: more than one latitude must be combined to get good resolution).

The wavelike regions are picked out quite well by large values of the parameter k/σ_k (this is even more apparent from animations than can be seen from comparison with snapshots). Waves in the core of the Circumpolar Current are seen to be eastward moving with speeds of 1 to 3 cm s^{-1} . This region corresponds well with the band of high and moderate variability seen in Plate 1b. Similar westward speeds are seen to the north of this band, west of South America and New Zealand, with speeds of less than 1 cm s^{-1} in both directions to the south. Wavelengths in the most wavelike regions are between 200 and 450 km, and periods range from about 4 months to a year, with longer periods in some of the southernmost regions. The following are some particular features.

A band of eastward moving waves stretches east and slowly south from the Agulhas Current region south of Africa. These waves have periods of slightly less than 6 months and wavelengths of about 350 km. Around 60°E, this band crosses the southern end of the Crozet Basin where Park and Saint-Guily detected very similar waves from Geosat altimetry [Park and Saint-Guily, 1992; Park, 1990]. Farther north in this basin they found westward propagating semiannual waves.

A wave moves westward from the southern tip of Tasmania, at a speed of about 3.5 cm s^{-1} . This wave has a well-defined wavelength (not shown) of about 800 km and is approximately annual.

A short period (about 4 months) disturbance is centered on 230°E, 55°S. This region corresponds approximately to the Eltanin fracture zone, which is somewhat surprising since the flow in FRAM is strongly concentrated through the nearby Udintsev fracture zone about 10 degrees farther west. Both fracture zones were also identified by Johnson *et al.* [1992] as regions of strong Reynolds stresses. The above features can all be clearly seen in animations of the original FRAM data, a fact which inspires confidence in the method of analysis.

6. Altimeter Results

Figure 5a shows that resolution of 1 month is, for the most part, capable of tracking the Rossby waves. The TOPEX/POSEIDON repeat period of just under 10 days should therefore resolve the waves quite easily. Spatial resolution is, however, more of a problem. The wavelength of the waves in FRAM is between about 3.75 and 5.5 degrees of longitude. The zonal spacing of crossover points in Figure 1 is $360/127 = 2.83$ degrees. This is enough to provide two points per wavelength only for the largest, southernmost waves, and that is only marginal resolution.

Fortunately, the waves are coherent over several degrees of latitude, and the diamond pattern of crossovers means that this fact can be used to effectively double the zonal resolution under favourable circumstances. The effect of this is shown in Figures 5b and 5c. Figure 5b is a time/longitude section of gradients derived from TOPEX/POSEIDON crossover points at 58.34°S. The eye of faith can just about discern wave activity at 290°E. In the lower figure, zonal resolution has been doubled by interpolating data from the neighbouring two latitudes onto the central latitude. Two areas of wave activity are now clearly seen, centered on 260°E and 290°E, and the waves look very similar to those seen in FRAM, with amplitudes of about 2 microradians. We may expect, then, that it is possible to resolve clearly the southernmost waves. As the crossovers get farther apart farther north, there must come a point where waves cannot be resolved.

The scheme used to extract wave parameters from the FRAM data is quite easy to adapt to the altimeter data. CPCs are calculated for patches of 19 crossover points from three latitudes (represented by dots in Figure 6). The first CPC for each region is then associated with

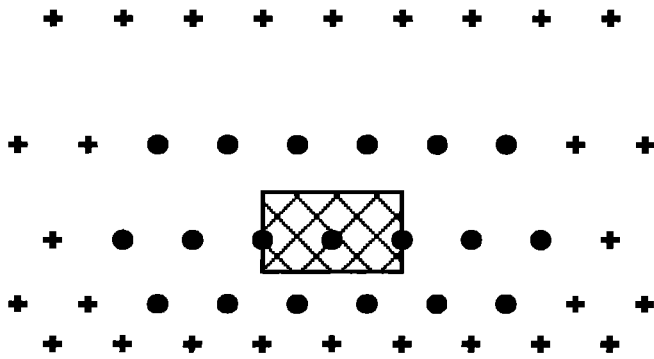


Figure 6. Schematic showing a patch of crossover points (dots) used to calculate a complex principal component, and the area associated with that component (hatched area) for purposes of plotting in Figure 3 and Plate 2.

an area of the FRAM grid corresponding to the center of the region (the cross-hatched area in Figure 6). The spatial part of the CPC is interpolated onto this grid, using a Gaussian relative weighting with scale length equivalent to 1.4 degrees of longitude and a cutoff at two scale lengths. Wavelength is then calculated from the central latitude. In order to assess the resolution attainable, this procedure was first employed on FRAM data sampled at crossover points. A reconstruction of the wave field is shown in Figure 3c demonstrating that south of about 55°S, the waves are resolved quite adequately. North of this latitude, although something of the waves is reproduced, the spatial structure is not properly resolved. This interpretation is reinforced by the wave parameters derived from this data set (Plate 2b), which show many fewer good values of the “wavelikeness” parameter, k/σ_k , and poor agreement with the full resolution wavelength and wave speed parameters north of this latitude. Wave period, however, is well reproduced over the whole region. This reflects the fact that the waves have coherence lengths of several wavelengths so, although the spatial phase structure is not resolved, the wave is still the dominant coherent structure over the region, and its temporal phase structure is adequately resolved.

TOPEX/POSEIDON data, processed as described in section 3, were subjected to the same principal component analysis as the subsampled FRAM data. A snapshot of the reconstructed wave field is shown in Figure 3d. While different in many details, there are some strong similarities to Figure 3c. Well-resolved waves are seen in the southeast Pacific sector, and strong, meridionally coherent structures are seen elsewhere along the core of the Circumpolar Current. Some of the more notable differences occur east of Drake Passage and south of Australia, where altimetry suggests more wavelike behaviour than that seen in FRAM, and south of the Tasman Sea, where FRAM produces a signature coherent over some 10 degrees of latitude, which is not seen in the altimetry.

The shape of the waves in the Pacific sector is of particular interest, and this region is shown magni-

fied in Figure 7. In both FRAM and in the TOPEX/POSEIDON reconstruction, individual wave trains seem to have a chevron-shaped structure, pointing along the direction of the mean flow. Figure 3 shows that this structure occurs in many places in FRAM, but that the resolution afforded by altimetry is only sufficient to reproduce it in the southeast Pacific sector. The Reynolds stresses produced by eddies of this shape [Wolff *et al.*, 1991] are in such a sense as to concentrate eastward momentum at the “arrow point”. If the deformation of the waves is caused by shear of the mean flow, this then acts as a positive feedback, reinforcing that shear.

As mentioned in the introduction, Reynolds stresses in the Southern Ocean (in both models and observations) are known to act in this sense, and distortion of Rossby waves by shear of the mean flow is a mechanism which has been proposed to explain this [Wolff *et al.*, 1991; McWilliams and Chow, 1981]. It is good then to see this chevron shape occurring in the real ocean.

Wave parameters derived from the altimeter data are shown in Plate 2c. Wavelike regions are found in similar places to the subsampled FRAM data, and with similar wavelengths. Eastward phase speeds in the Pacific sector are mostly in the 1 to 4 cm s^{-1} range. There are interesting differences in this region though. In the altimeter data, a patch of westward moving waves is seen south of about 60°S, and short period (about 4 months) waves are visible (and very clearly seen in animations) passing through the northern half of Drake Passage at speeds of up to 4 or 5 cm s^{-1} . Such a discrepancy is not particularly disturbing since the southeast Pacific is a very poorly sampled region of the ocean, so Levitus data here is strongly smoothed. A concentration of the mean flow into a stronger jet, north of 60°S is entirely plausible and would explain the difference well.

Curiously, waves with westward phase speeds are much more common in the altimetry, south of the main current. Virtually no westward phase speeds faster than 1 cm s^{-1} are seen in the FRAM data, south of the Circumpolar Current, but phase speeds of -1 to -5 cm s^{-1} are common in the altimetry and occur in many of the regions identified as wavelike. This may indicate an underrepresentation of Rossby waves by the model in these regions. The first internal Rossby radius can be as small as 10 km this far south, so the problem may be simply one of lack of resolution.

Perhaps the most interesting of the parameters is the wave period, which was shown from the FRAM data to be insensitive to spatial resolution. There are regions of significant agreement with FRAM, in particular: (1) near-annual waves in the north-eastern part of the Pacific sector, (2) short period waves in the region of the Eltanin fracture zone, (3) the band of near-semiannual waves stretching eastward and slowly south from the Agulhas current region, and (4) near-semiannual waves appear to comprise a large part of the remaining Pacific sector of the Circumpolar Current.

Shallow regions and less energetic regions of the ocean (see Plate 1a and Figure 2) show short period variability (1.5- to 4.5-month periods, shown in light and dark

FRAM full resolution wave parameters

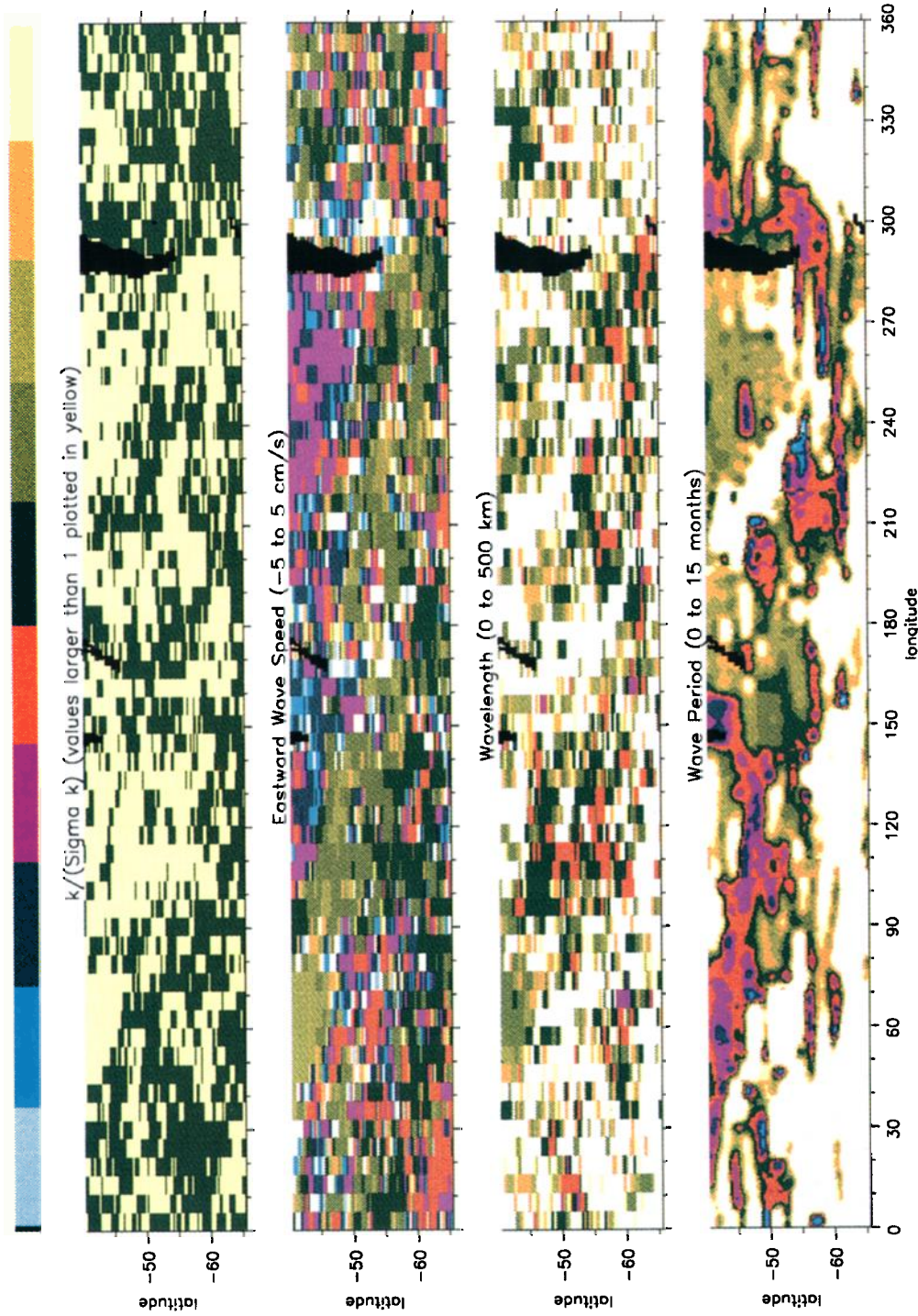


Plate 2. Wave parameters derived from local complex principal component representations of the zonal gradient of sea surface height. Each group contains (1) k/σ_k , a measure of the “wavelikeness” of the field, (2) the best fit speed of the wave, eastward being measured as positive, (3) best fit wavelength, and (4) best fit wave period (slight smoothing makes wave period easier to interpret, other parameters do not benefit from smoothing). White regions are where the plotted quantity is off the scale specified in the title, (a) derived from 4 years of monthly FRAM data, (b) the same as Plate 2a but using only FRAM data sampled at TOPEX/POSEIDON crossover points, (c) the same as Plate 2b but using TOPEX/POSEIDON measurements, (d) the same as Plate 2b but using the difference between two tide models as sampled by TOPEX/POSEIDON (note the different scales).

FRAM sub-sampled wave parameters

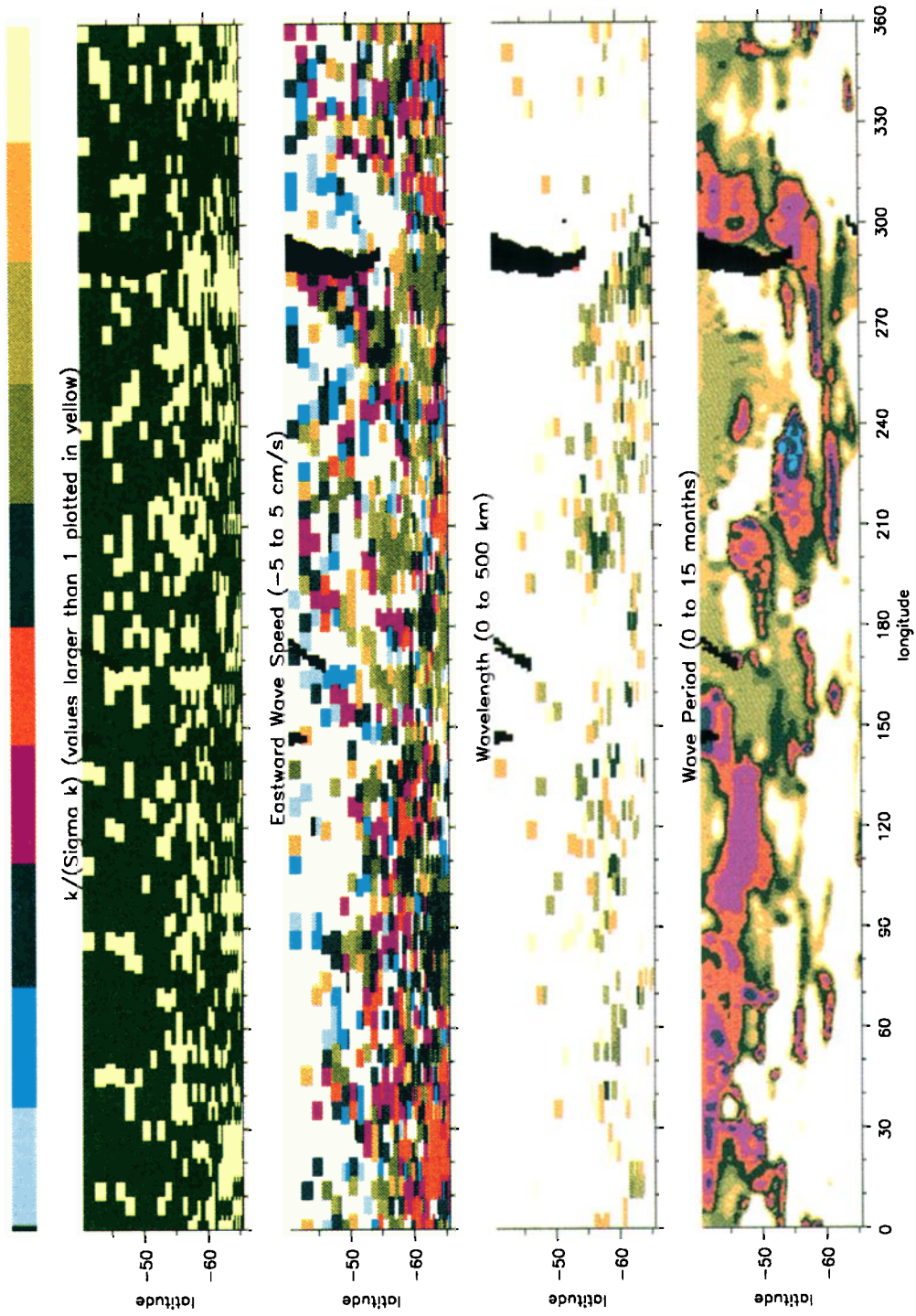


Plate 2. (continued)

Topex/Poseidon wave parameters



Plate 2. (continued)

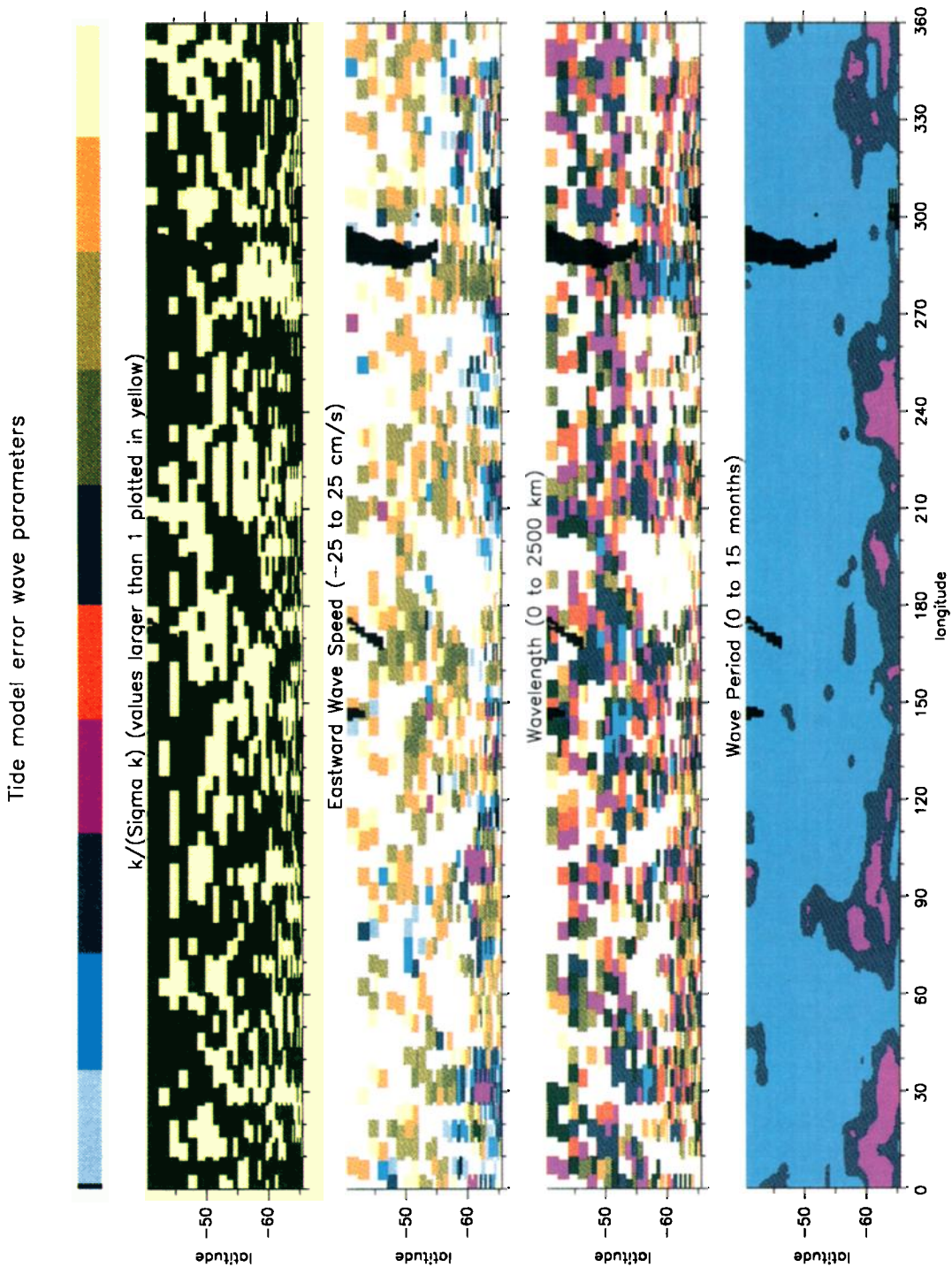


Plate 2. (continued)

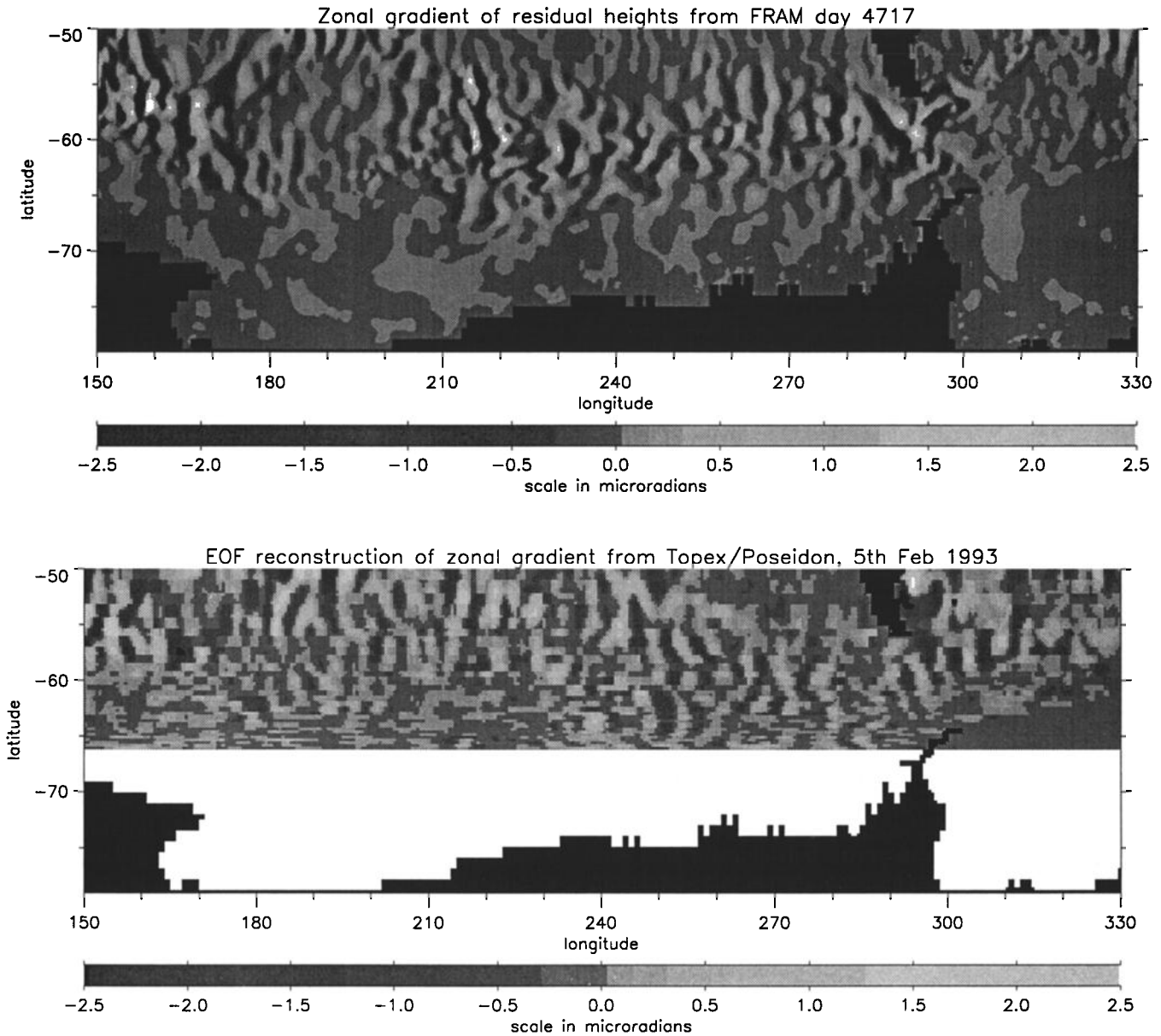


Figure 7. Expanded views of regions from (a) Figure 3a, and (b) Figure 3d.

blue). These are regions where tide model error is likely to be significant, and the next section demonstrates that such errors can explain these features. In other regions of disagreement, particularly between 300°E and 360°E and in a broad region surrounding New Zealand, altimetry gives shorter periods than FRAM. This might be interpreted as being due to the lack of high-frequency forcing in FRAM, but a more plausible explanation may be due to resolution. FRAM only resolves the first internal Rossby radius, and that is barely resolved. Even so, the most energetic regions in FRAM are often associated with shorter periods and wavelengths. It may be that the limited resolution is preventing the propagation of these short period eddies into quieter regions, thus leaving the longer period signal dominant in these regions.

7. Tide Model Errors

Typical mid-ocean tidal slopes are around $0.2\ \mu\text{rad}$, or about an order of magnitude smaller than the signals considered here. This is one of the advantages of considering slopes rather than heights, since mid-ocean tides have length-scales of thousands of kilometres. Nonetheless, it is possible that errors in the tidal model could have larger slopes over localised regions, and the strange sampling of tides by an orbiting altimeter produce aliasing effects which can simulate a wide variety of wave motions [Schlax and Chelton, 1994]. Fortunately with TOPEX/POSEIDON sampling, the M_2 , S_2 , and O_1 tides have aliased periods of 62.1, 58.8, and 45.7 days, respectively [Knudsen, 1995], and so are quite distinct from the longer period signals examined here. All these

periods fall in the 1.5- to 3-month band represented in mid-blue in Plate 2. Also important in the Southern Ocean is the K_1 tide, which is aliased to 173.3 days, or just under 6 months. This would appear to be more of a problem, but the spatial aliasing of the K_1 tide is more helpful. Neighbouring passes sample the K_1 tide with phases separated by only 9 degrees, and the phase difference between ascending and descending passes disappears at about 50°N and 50°S [Knudsen, 1995]. As a result, K_1 tides will not be aliased to higher wavenumbers, and confusion with Rossby waves should not generally result.

In order to check these ideas, an ocean tide model error field was produced by producing files of differences between the *Cartwright and Ray* [1991] tides and the *Eanes* [1994] tides, as sampled by TOPEX/POSEIDON, and these were processed in the same manner as the residual height data to produce a tidal error version of the residual gradients. Figure 8 shows a map of the root-mean-square residual gradients from the tide error data, which can be compared with Figure 2 to show that tide errors make a small contribution to the signal except in shallow areas (note the different scales). This inspires confidence that tide model errors are not a significant factor in the present analysis, the Cartwright and Ray model being derived from Geosat altimetry and the Eanes model from completely independent TOPEX/POSEIDON information. It should be noted though, that the difference between these two models has a resolution of 3 degrees, so errors in the Cartwright and Ray model on shorter length scales than this are not accounted for.

A principal components analysis of the tide error data produces the wave parameters shown in Plate 2d (note the different scales). Although a good “wavelikeness”

is produced in some regions, the wave speed is never less than 5 cms^{-1} ; the wavelengths are too long and the wave periods are only a problem in a few small regions. Even in the worst case, tide model errors cannot interfere with the detection of Rossby waves, although it is clear that much of the short period activity seen in Plate 2c is probably due to tide model error.

8. Conclusions

Rossby waves modelled in FRAM show several interesting properties. They occur at a natural scale of approximately 300 km, and in two distinct regimes: within the core of the Circumpolar Current they show strong interaction with the mean flow and are advected eastward with the current; outside this region they are more nearly linear and travel westward. This suggests that the Southern Ocean might instructively be divided into two separate dynamical regimes in which the flow is, respectively, subcritical and supercritical with regard to the speed of propagation of these waves.

The eastward travelling waves have larger amplitudes (about 2 microradians, measured in terms of the zonal gradient of sea surface) and tend to be chevron-shaped, pointing along the direction of the mean flow, a fact which is consistent with their acting to accelerate the eastward flowing jets.

TOPEX/POSEIDON altimetry data has been shown to be consistent with the existence of these waves in parts of the Southern Ocean, and actually resolves their spatial structure in the southeast Pacific sector. Here the chevron-shaped structure is seen to occur in the real ocean. An analysis of tide model errors shows that they are not important to the interpretation of the waves, although they probably explain some of the discrepan-

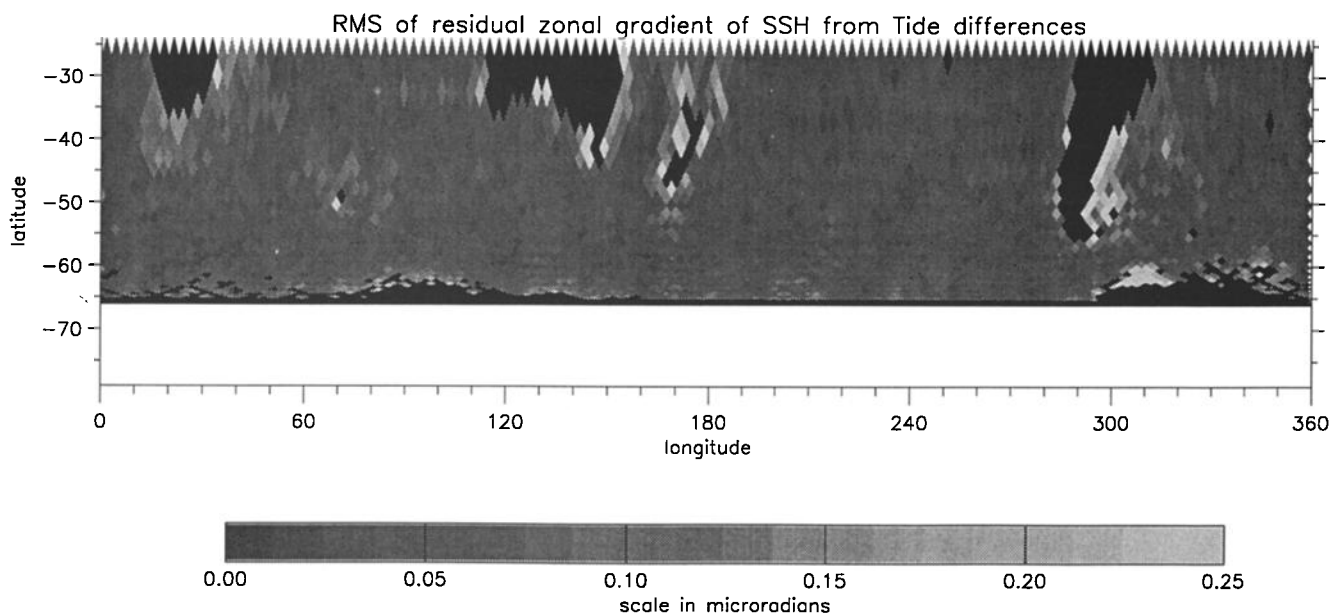


Figure 8. Root-mean-square variability of the component of zonal gradient of sea surface height produced by the difference between two tide models, calculated in the same way as Figure 2 (note the different scale).

cies observed in shallow and in less energetic regions of the Southern Ocean. Other differences between altimetry and model results, especially for wave periods, may be more significant. In particular, short period (semiannual and shorter) waves seem to spread farther from the high-energy regions in the altimetry, and waves with westward phase speed south of the main current are much more common in the altimetry than in the model. Differences in the southeast Pacific sector may indicate that the real current forms a narrower jet than the modelled current in this region, on a level with the northern half of Drake Passage.

It should be emphasised that the interpretation of these signals as Rossby waves relies on the agreement with model data. Uncertainties in the mean flow of the real Circumpolar Current preclude the use of dispersion relations to confirm the identity of the waves, although their period and wavelength are certainly plausible for Rossby waves in these circumstances. The model predicts waves throughout the core of the Circumpolar Current, but also predicts that they should only be spatially resolved by TOPEX/POSEIDON altimetry in the southeast Pacific. Altimetry indeed resolves similar-looking waves only in this sector, but produces wave periods consistent with model results in several significant regions. Differences between model and altimetry are also significant, however, and an unambiguous interpretation of the data must await a dynamical theory of the Circumpolar Current which can explain both the similarities and the differences. Nonetheless, Figure 7 provides compelling evidence for the presence of Rossby waves, at least in the southeast Pacific sector of the Circumpolar Current, if any credence at all is given to the model results.

A crucial factor limiting this analysis has been the poor spatial resolution afforded by the crossover points of the TOPEX/POSEIDON altimeter. Crossover points for the ERS altimeters, when in a 35-day repeat orbit, are separated by 0.72 degrees of longitude, which would be adequate to resolve waves much farther north. The disadvantage of ERS data is the relatively poor temporal resolution. Some waves will only be marginally resolved in time by the ERS altimeters, and the 17 days which pass between the ascending and descending passes at certain crossover latitudes may prove too much for a meaningful reconstruction of the zonal component of sea surface slope. Nonetheless, work is underway to perform a similar analysis on ERS 1 data, and it is hoped that it will prove possible to use the spatial resolution from ERS 1 together with the temporal resolution from TOPEX/POSEIDON to define these waves clearly over the entire Southern Ocean.

Acknowledgments. This work was funded partly by the U.K. Defence Research Agency and the U.K. Natural Environment Research Council.

References

- AVISO, AVISO User Handbook: Merged TOPEX/POSEIDON Products, *Rep. AVI-NT-02-101-CN*, 2nd ed., CNES, Toulouse, France, 1992.
- Barnett, T.P., Interaction of the monsoon and Pacific trade wind system at interannual time scales, I, The equatorial zone, *Mon. Weather Rev.*, *111*, 756–773, 1983.
- Cartwright, D.E., and R.D. Ray, Energetics of global ocean tides from Geosat altimetry, *J. Geophys. Res.*, *96*(C9) 16,897–16,912, 1991.
- Chelton, D.B., M.G. Schlax, D.L. Witter, and J.G. Richman, Geosat Altimeter Observations of the Surface Circulation of the Southern Ocean, *J. Geophys. Res.*, *95*(C10), 17,877–17,904, 1990.
- Cox, M.D., A primitive equation, three-dimensional model of the Ocean, *GFDL Ocean Group Tech. Rep. 1*, Geophys. Fluid Dyn. Lab./NOAA, Princeton University, Princeton, N. J., 1984.
- Eanes, R.J., Diurnal and semidiurnal tides from TOPEX/POSEIDON altimetry, *Eos Trans. AGU*, *75*(16), 108, Spring Meet. suppl., 1994.
- Fine Resolution Antarctic Model (FRAM) Group, An eddy-resolving model of the Southern Ocean, *Eos Trans. AGU*, *72*(17), 169–175, Spring Meet. suppl., 1991.
- Gaspar, P., F. Ogor, P.Y. LeTraon, and O.Z. Zanife, Estimating the sea-state bias of the TOPEX and POSEIDON altimeters from crossover differences, *J. Geophys. Res.*, *99* 24,981–24,994, 1994.
- Gill, A.E., *Atmosphere-Ocean Dynamics*, 662pp, Academic, San Diego, Calif., 1982.
- Greatbatch, R.J., A note on the representation of steric sea level in models that conserve volume rather than mass, *J. Geophys. Res.*, *99*(C6), 12,767–12,771, 1994.
- Hellerman, S., and M. Rosenstein, Normal monthly wind stress over the world ocean with error estimates, *J. Phys. Oceanogr.*, *13*, 1093–1104, 1983.
- Johnson, T.J., R.H. Stewart, C.K. Shum, and B.D. Tapley, Distribution of Reynolds stress carried by mesoscale variability in the Antarctic Circumpolar Current, *Geophys. Res. Lett.*, *19*(12), 1201–1204, 1992.
- Killworth, P.D. and M.M. Nanneh, Isopycnal momentum budget of the Antarctic circumpolar Current in the fine resolution antarctic model. *J. Phys. Oceanogr.*, *24*, 1201–1223, 1994.
- Knudsen, P., Global Low Harmonic Degree Models of the seasonal variability and residual ocean tides from TOPEX/POSEIDON altimeter data, *J. Geophys. Res.* *99*, 24,643–24,655, 1995.
- Levitus, S., Climatological atlas of the world ocean, *NOAA Prof. Pap.*, *13*, 173, 1982.
- McWilliams, J.C., and J.M.S. Chow, Equilibrium geostrophic turbulence, I, A reference solution in a β -plane channel, *J. Phys. Oceanogr.*, *11*, 921–949, 1981.
- Morrow, R., J. Church, R. Coleman, D. Chelton, and N. White, Eddy momentum flux and its contribution to the Southern Ocean momentum balance, *Nature*, *357*, 482–484, 1992.
- Morrow, R., R. Coleman, J. Church, and D. Chelton, Surface eddy momentum flux and velocity variances in the Southern Ocean from Geosat altimetry, *J. Phys. Oceanogr.*, *24*, 2050–2071, 1994.
- Nouel, F., J.P. Berthias, M. Deleuze, P. Laudet, A. Piuze, D. Pradines, C. Valorge, C. Dejoie, M.F. Susini, and D. Taburiau, Precise CNES orbits for TOPEX/POSEIDON: Is reaching 2 cm still a challenge?, *J. Geophys. Res.* *99*, 24,405–24,419, 1995.
- Nowlin, W.D., Jr., and J.M. Klinck, The Physics of the Antarctic Circumpolar Current, *Rev. Geophys.*, *24*(3), 469–491, 1986.
- Park, Y.-H., Mise en évidence d'ondes planétaires semi-annuelles baroclines au Sud de l'Océan Indien par altimétrie satellitaire, *C. R. Acad. Sci. Paris*, *310*, II, 919–926, 1990.
- Park, Y.-H., and B. Saint-Guilly, Sea level variability in the Crozet-Kerguelan-Amsterdam area from bottom pressure

- and Geosat altimetry, in *Sea Level Changes: Determination and Effects*, *Geophys. Monogr. Ser.*, vol.69, IUGG vol.11, edited by P.L. Woodworth, D.T. Pugh, R.G. Warwick, and J. Hannah, 196 pp., AGU, Washington, D. C., 1992.
- Rapp, R.H., Y. Wang, and N.K. Pavlis, The Ohio state 1991 geopotential and sea surface topography harmonic coefficient models, *Rep. 410*, Dept. of Geod. Sci. and Surv., Ohio State Univ., Columbus, Ohio, 1991.
- Rhines, P.B., Edge- bottom- and Rossby waves in a rotating stratified fluid, *Geophys. Fluid Dyn.*, 1, 273-302, 1970.
- Saunders, P.M., and S.R. Thompson, Transport, heat, and freshwater fluxes in a diagnostic numerical model (FRAM), *J. Phys. Oceanogr.*, 23(3), 452-464, 1993.
- Schlax, M. G., and D. Chelton, Detecting aliased tidal errors in altimeter height measurements, *J. Geophys. Res.*, 99(C6), 12,603-12,612, 1994.
- Semtner, A.J., and R.M. Chervin, Ocean general circulation from a global eddy-resolving model, *J. Geophys. Res.*, 97(C4), 5493-5550, 1992.
- Shum, C.K., R.A. Werner, D.T. Sandwell, B.H. Zhang, R.S. Nerem, and B.D. Tapley, Variations of Global Mesoscale Eddy Energy Observed From Geosat, *J. Geophys. Res.*, 95(C10), 17,865-17,876, 1990.
- Stevens, D.P., and P.D. Killworth, The distribution of kinetic energy in the Southern Ocean. A comparison between observations and an eddy resolving general circulation model, *Philos. Trans. R. Soc. London B*, 338, 251-257, 1992.
- Treguier, A.M., and J.C. McWilliams, Topographic influence on wind-driven stratified flow in a β -plane channel: An idealised model for the Antarctic Circumpolar Current, *J. Phys. Oceanogr.*, 20, 321-343, 1990.
- Wolff, J.-O., D. Olbers, and E. Maier-Reimer, Wind-driven flow over topography in a zonal β -plane channel: A quasi-geostrophic model of the Antarctic Circumpolar Current, *J. Phys. Oceanogr.*, 21, 236-264, 1991.
-
- C. W. Hughes, Proudman Oceanographic Laboratory, Bidston Observatory, Birkenhead, Merseyside, L43 7RA, U.K. (e-mail: C.Hughes@pol.ac.uk)

(Received August 19, 1994; revised January 23, 1995; accepted April 6, 1995.)